EUROPEAN ORGANIZATION FOR NUCLEAR RESEARCH

CERN-EP/88-170
November 30th, 1988

# PRODUCTION OF PSEUDOSCALAR MESONS IN 300 GEV CENTRAL $\pi^-$N COLLISIONS

IHEP[1] – IISN[2] – LANL[3] – LAPP[4] – Pisa[5] Collaboration

(Joint CERN – IHEP experiment)

D.Alde [3], R.Bellazzini [5], F.G.Binon [2,6], M.Boutemeur [4], A.Brez [5], C.Bricman [2,6], S.V.Donskov [1], M.Gouanère [4], A.V.Inyakin [1], V.A.Kachanov [1], G.V.Khaustov [1], E.A.Knapp [3], A.V.Kulik [1], A.A.Lednev [1], M.M.Massai [5], L.Massonnet [4], J.P.Peigneux [4], Yu.D.Prokoshkin [1], S.A.Sadovsky [1], V.D.Samoylenko [1], P.M.Shagin [1], A.V.Shtannikov [1], A.V.Singovsky [1], J.P.Stroot [2,6], V.P.Sugonyaev [1] and M.R.Torquati [5]

## Abstract

The exclusive production of $\pi^0$, $\eta$ and $\eta'$ mesons in $\pi^-$N central collisions has been studied with 300 GeV incident pions. The experiment has been performed at the CERN SPS. The gammas from decaying mesons were detected in the hodoscope multiphoton spectrometer GAMS – 4000. The measured differential cross sections show a plateau in the longitudinal momentum interval $0.1 < x_F < 0.3$.

---

[1] Institute for High Energy Physics, Serpukhov, USSR.
[2] Institut Interuniversitaire des Sciences Nucléaires, Belgium.
[3] Los Alamos National Laboratory, New Mexico, USA.
[4] Laboratoire d'Annecy de Physique des Particules, France.
[5] University of Pisa and INFN, Italy.
[6] Mailing address : CERN, EP Division, 1211 Geneva 23, CH.

## 1. Introduction

The first experimental data on the production of pseudoscalar mesons in the central region of the collision of pions on nucleons have been obtained in a study of the exclusive reaction

$$\pi^- N \to \pi^- N P^0 \qquad (1)$$

with a 300 GeV/c pion beam from the CERN SPS incident on an active scintillator target. $P^0$ mesons are the lightest neutral non-strange pseudoscalar mesons : $\pi^0$, $\eta$ or $\eta'$.

The region of central collisions in reaction (1) is characterised by the following kinematical constraints [1], [2] :

- the meson $P^0$ is produced with small momentum in the c.m. system : $x_F$ and $p_T \approx 0$, as a cluster in the central region of the rapidity distribution;

- the pion and the nucleon, after collision, have momenta close to their initial values : $|x_F| > 0.8$ and $p_T \approx 0$.

The basic mechanism of such processes is double Reggeon exchange [1], [2] Previous experiments [2] - [6] show that inelastic diffraction, in which either hadron may be excited, is the main competing process. It is strongly suppressed by imposing a sufficiently large gap in rapidity between the leading particles and the central cluster.

There is no reliable theoretical evaluation of Reggeon − Reggeon interaction. It is difficult on one hand and existing data are few.

## 2. Experimental setup

The experimental setup (Fig. 1) has been described in earlier studies of the central production of scalar and tensor mesons in a search for glueballs [7], [8]. The pseudoscalar mesons have been measured in reaction (1) through their decay into gammas by GAMS − 4000, a multiphoton lead-glass electromagnetic calorimeter [9] - [13].

A magnetic spectrometer, composed of three bending magnets with a total bending power of 9 T·m and of four multi-wire proportional chambers (MWPC) with a 2 mm pitch, measures with a resolution of 5 GeV/c the momentum of the forward particles, which pass through the central hole of GAMS. The last detector of the spectrometer is a 9 – cell modular hadron calorimeter MHC – 9 [14], [15] which independently from MWPC measures the momentum and coordinates of the forward emitted $\pi^-$ and allows to eliminate the muon background, particularly from pions decaying in flight.

The production target is active. It is made of 16 pieces of 5 mm thick plastic scintillator spaced at 25 mm intervals and each coupled to a photomultiplier. It is surrounded by a cylindrical guard system made of a layer of scintillators and a layer of lead-glass counters. The guard system is used to suppress inelastic processes.

The first level trigger depends on all following conditions being simultaneously satisfied :

– a fast coincidence between beam counters $S_1$ to $S_4$, the last being the first counter of the active target;

– one and only one particle in the MWPCs of the forward magnetic spectrometer;

– the momentum of this particle does not exceed 285 GeV/c as evaluated by the MWPC fast processor;

– there is no signal in the counters AH as well as in the aperture defining sandwich counters, so that only neutral particles emitted inside the target may be detected in GAMS;

– the energy released in GAMS, measured by a fast adder of the dynode signals of GAMS, is larger than 10 GeV in first approximation;

– more than 100 GeV energy is released in MHC – 9.

A second level trigger is made by a fast processor linked to the output of the ADC system providing a higher accuracy threshold of 7 GeV for $E_{GAMS}$, the total energy released in GAMS [10], [13].

The trigger is sufficiently loose in order to accept all processes involved in central production. It places the following limits on the longitudinal Feynman momentum of the detected particles : $x_F >$

0.5 for the outgoing $\pi^-$, $x_F < -0.8$ for the recoiling protons or $x_F < -0.7$ for the neutrons. The limit on $x_F$ for $P^0$ depends on its mass and on the total energy threshold in GAMS. A threshold of 7 GeV corresponds to $x_F = 0$ for $\eta$. Stronger selection criteria are applied at the stage of off-line data treatment.

## 3. Data treatment

Ten million events from reaction (1) have been written on tape. The first step in the analysis is to check the energy balance of each event : $E_{tot} = E_{GAMS} + E_\pi = (300 \pm 10)$ GeV (Fig. 2) $E_\pi$ is the forward pion energy measured with the magnetic spectrometer. In order to enhance central collision detection, $P^0$-systems are chosen in the rapidity interval $0 < y < 2$ (for $y < 0$, the acceptance of the setup is zero).

Photon energy and coordinates are determined through shower reconstruction programs that classify events according to their gamma multiplicity [10], [12]. $\pi^0$ and $\eta$ are found in the $2\gamma$ events, $\eta$ and $\eta'$ in the $6\gamma$ events. A total of $3 \cdot 10^5$ $2\gamma$ events and $1.2 \cdot 10^5$ $6\gamma$ events have been collected.

Events with $3\gamma$ and $4\gamma$ have also been analysed. There are no peaks seen in the $3\gamma$ mass spectrum in the region of $\pi^0$, $\eta$ or $\eta'$. There is thus no spurious gamma contribution in the data [16]. Similarly, no peak is observed in the same $3\gamma$ spectrum at the mass of f(1270) which appears in the $4\gamma$ spectrum. Thus the number of events with missing gammas is also negligeable.

Reconstructed events are then submitted to a kinematical fit and to an optimization procedure that depends on the observed decay. Final results are obtained by taking into account the setup acceptance, the selection criteria and the reconstruction efficiency, determined by a Monte Carlo simulation using the same procedures as for experimental data.

## 4. Neutral pions

Neutral pions produced in reaction (1) are detected by their $2\gamma$ decay channel. The invariant mass spectrum of $\gamma$-pairs after a 1C fit ($E_{tot}$ = 300 GeV) is dominated by a $\pi^0$ peak (Fig. 3). The background under the peak is less than 20 %. The angular distribution of events in the peak is uniform, taking into account detection efficiency, as expected for a spinless particle (Fig. 4).

The background from the reaction $\pi^- N \rightarrow \rho^- N$ with $\rho^-$ decaying into $\pi^-\pi^0$ has been evaluated from the $\pi^-\pi^0$ mass spectrum. There is no visible structure at the $\rho$ mass. Most events in this spectrum have masses larger than 1.5 GeV.

The influence of the photon energy threshold in GAMS on the number of events agrees with the evaluated $\pi^0$ detection efficiency in reaction (1) (Fig. 5).

The low momentum recoil protons are usually absorbed in the scintillator of the production target. Such events are identified by requiring the signal of one of the live target counters to be larger than twice that of a minimum ionizing particle. They comprise one quarter of the total number of events, but the background is reduced by an order of magnitude (Fig. 3b). The background under the total energy peak is similarly supressed (Fig. 2d). This cut however does not alter the shape of the distributions. It is not applied in subsequent data (Fig. 4 and seq.).

## 5. $\eta$ mesons

Eta production has been studied by detecting it through its two most abundant neutral decay modes : $2\gamma$ and $3\pi^0 \rightarrow 6\gamma$. The $\eta$ search amongst $2\gamma$ events is similar to that for $\pi^0$ described above (Fig. 6). The angular distribution of events in the $\eta$ peak is as expected from a spinless particle. The number of events varies with the detection energy threshold in agreement with efficiency evaluations (Fig. 5).

Identification of the $\eta$ from $6\gamma$ events is more delicate, as the mean photon energy is reduced by a factor three in comparison with that of $2\gamma$ events. A 4C fit with fixed mass for each particle in the final

state is required to have a C.L. larger than 0.1 before further analysis (Fig. 7). Again, there is good agreement in the variation of the number of accepted events and the evaluated efficiency with energy threshold (Fig. 5).

The quality of the identification procedure is confirmed by the good agreement between the value of the slope of the square of the linear matrix element of the $3\pi^0$ decay measured on the Dalitz plot (Fig. 8a) and that obtained in a former high precision experiment [17]. An overall consistency check is provided by the equality of the numbers of $2\gamma$ and $6\gamma$ events after correction for detection efficiency (40 % and 6 %, respectively) taking into account partial decay widths and photon absorption in the production target. Their ratio is $0.96 \pm 0.08$.

As it was already the case for $\pi^0$, the mass spectra of the combinations of the $\pi^-$ with the particles of the central cluster ($\pi^-\eta$, $\pi^-\pi^0$, $\pi^-\pi^0\pi^0$) do not show any significant structure, most events having a mass larger than 1 GeV.

## 6. $\eta'$ mesons

The $2\gamma$ decay of $\eta'$ is not visible above the background in the $2\gamma$ mass spectrum produced in reaction (1). On the other hand $\eta'$ are observed in the more complicated topology of $6\gamma$ events through the decay $\eta' \rightarrow \eta\pi^0\pi^0$. A peak is seen at the $\eta'$ mass in the spectrum of $6\gamma$ events which have passed a 4C fit (Fig. 9).

The agreement of the dependence of the square of the matrix element on the Dalitz variables measured in the present reaction with that of the former precise specific experiment on that decay [18] is a check of the procedure of identification (Fig. 8b).

## 7. Production cross – sections

The distributions of the square of $p_T$, the transverse momentum of the final state particles, $\pi^-$, N and $P^0$, are identical for all $P^0$ ($\pi^0$, $\eta$ and $\eta'$). Events are concentrated in the small $p^2_T$ region ($p^2_T < 1$ (GeV/c)$^2$). The vectors $\vec{p}_T(\pi^-)$ and $\vec{p}_T(P^0)$ are measured directly. The $\vec{p}_T$ value of the recoil nucleon is deduced by momentum balance : $-\vec{p}_T(N) = \vec{p}_T(\pi^0) + \vec{p}_T(P^0)$. There is no correlation between $\vec{p}_T(N)$ and $\vec{p}_T(\pi^-)$. This reflects the fact that Reggeons are emitted indepently at each vertex of the double Reggeon diagram.

Longitudinal momentum distributions are displayed on Fig. 11 together with detection efficiency. Differential cross sections for the central production of $\pi^0$ and $\eta$ have been determined from the above data, taking into account the target absorption of photons and of $\pi^-$, the effective number of nucleons in the scintillator of the live target being scaled down by a factor $A^{2/3}$ [7] (Fig. 12).

The cross sections $d\sigma/dx_F$ are practically constant for $x_F$ above 0.05 up to 0.3. The possible raise at very low $x_F$, at least for $\pi^0$, is not conclusive because the detection efficiency drops very fast in this region (Fig. 11).

The systematic errors are minimized in determining cross section ratios by comparing the number of events in processes which involve events with the same photon multiplicity. In the plateau region of $x_F$ (Fig.12) :

$$\frac{d\sigma(\pi^- N \to \pi^- N \pi^0)/dx_F}{d\sigma(\pi^- N \to \pi^- N \eta)/dx_F} = 12 \pm 2 \qquad (2)$$

(for $2\gamma$ events, $0.05 < x_F < 0.20$) and

$$\frac{d\sigma(\pi^- N \to \pi^- N \eta)/dx_F}{d\sigma(\pi^- N \to \pi^- N \eta')/dx_F} = 3 \pm 1 \qquad (3)$$

(for $6\gamma$ events, $0.05 < x_F < 0.30$).

## 8. Conclusion

The exclusive production of $\pi^0$, $\eta$ and $\eta'$ mesons have been studied for the first time in $\pi^-$N central collisions. The measured differential cross sections show a plateau in the domain $0.1 < x_F < 0.3$.

The authors would like to thank the CERN and IHEP directorates for their support to the GAMS programme. They also would like to acknowledge the technical assistance of T.Lopez and D.Michotte.

### References

[1] Yu.A.Azimov et al., Yad.Fiz. 21 (1975) 413.

[2] B.R.Desai et al., Nucl. Phys. 142B (1978) 258.

[3] M.Derrick et al., Phys.Rev. D4 (1974) 1215.

[4] T.Akesson et al., Phys.Lett. 133B (1983) 268.

[5] R.Waldi et al., Zeit. Phys. C18 (1983) 301.

[6] T.A.Armstrong et al., Phys. Lett. 167B (1986) 133.

[7] D.Alde et al., Phys. Lett. 201B (1988) 160; Yad. Fiz. 47 (1988) 1639.

[8] D.Alde et al., Yad. Fiz. 47 (1988) 1273.

[9] D.Alde et al., Nucl. Phys. B269 (1986) 485; Yad. Phys. 44 (1986) 120.

[10] D.Alde et al., CERN preprint EP 87 – 28 (1987).

[11] F.Binon et al., Nucl.Instr.Meth. A248 (1986) 86.

[12] A.V.Kulik et al., IHEP preprint 85 – 17, Serpukhov (1985).

[13] D.Alde et al., Nucl.Instr.Meth. A240 (1986) 343.

[14] V.S.Datsko et al., IHEP preprint 87 – 85, Serpukhov (1987).

[15] F.Binon et al., Nucl.Instr.Meth. A256 (1987) 444.

[16] F.Binon et al., Nuovo Cim. 71A (1982) 497; Yad.Fiz. 36 (1982) 670.

[17] D.Alde et al., Zeit.Phys. C25 (1984) 225; Yad.Fiz. 40 (1984) 1447.

[18] D.Alde et al., Phys.Lett. 177B (1986) 115; Yad.Fiz. 45 (1987) 117.

FIGURE CAPTIONS.

Fig.1 Experimental setup. $S_{1-5}$ : scintillation counters; $H_{1,2}$ : hodoscopes with a 1 mm step; T: live target; A, AH: scintillation counters; GS: lead-glass counters; $SW_{1,2}$ : aperture defining sandwich counters; GAMS − 4000: hodoscope lead-glass spectrometer; MHC − 240 and MHC - 9 : modular hadron calorimeters; $M_{1-3}$ : magnets; $MWPC_{1-4}$ : multiwire proportional chambers of the magnetic spectrometer; GAMS − 64: electromagnetic calorimeter allowing to detect the photons passing through the central hole in GAMS − 4000.

Fig.2. a) Energy spectrum of the $\pi^-$ mesons measured with the magnetic spectrometer. b) Distribution of events versus the total energy released by photons in GAMS − 4000. c) Spectrum of $E_{tot} = E_\pi + E_{GAMS}$ (shaded part is the distribution of $\eta \to 3\pi^0$ events, histogram bin: 20 MeV). d) same as in Fig.2c but when the live target has detected a recoiling proton.

Fig.3. Invariant mass spectra of gamma pairs: a) all events, b) a recoiling proton has been detected in the live target. The arrows point to the tabulated value of the $\pi^0$ mass (bin width: 5 MeV).

Fig.4. Angular distribution of events in the region of the $\pi^0$ peak. $\theta^*$ is the angle in the $P^0$ rest frame between the momentum vector of one of the photons and the momentum vector transfered by the $\pi^-$ ("Reggeon momentum"). The Monte Carlo distribution for the decay $\pi^0 \to 2\gamma$ is in good agreement with the measured one.

Fig.5. Dependence of the number of detected $\pi^0$ and $\eta$ on the threshold energy in GAMS − 4000. The curves are the computed efficiencies (normalized to the experimental data at $E_{th} = 0$).

Fig.6. Same as in Fig.3 but for events in the region of the $\eta$ peak (bin width: 10 MeV).

Fig.7. Invariant mass spectrum of $3\pi^0$ systems. The dashed curve is a polynomial fit of the background.

Fig.8. a) Dependence of the matrix element squared for the decay $\eta \to 3\pi^0$ on the variable $z = (r/r_{max})^2$, where r is the distance to the center of the Dalitz plot. The straight line is the result of a

high precision measurement [17]. b) Dependence of the matrix element squared of the decay $\eta' \rightarrow \eta\pi^0\pi^0$ on Dalitz variables. The straight lines are the result of measurements [18].

Fig.9. Invariant mass spectrum of $\eta\pi^0\pi^0$-systems. The arrow points to the tabulated mass value of the $\eta'$ meson. The full curve is the result of a fit. The dashed curve is a polynomial background.

Fig.10. Distribution of the events in reaction (1) versus the transverse momentum squared of the leading particles ($\pi^-$,N) and of the central cluster ($P^0 = \pi^0$). The distributions are the same for $P^0 = \eta$, $\eta'$.

Fig.11. Distribution of events in various channels of reaction (1) versus $x_F$. The dashed curve is the detection efficiency $\varepsilon$.

Fig.12. Differential cross sections of the reactions $\pi^- N \rightarrow \pi^- N\, \pi^0$ and $\pi^- N \rightarrow \pi^- N\, \eta$.

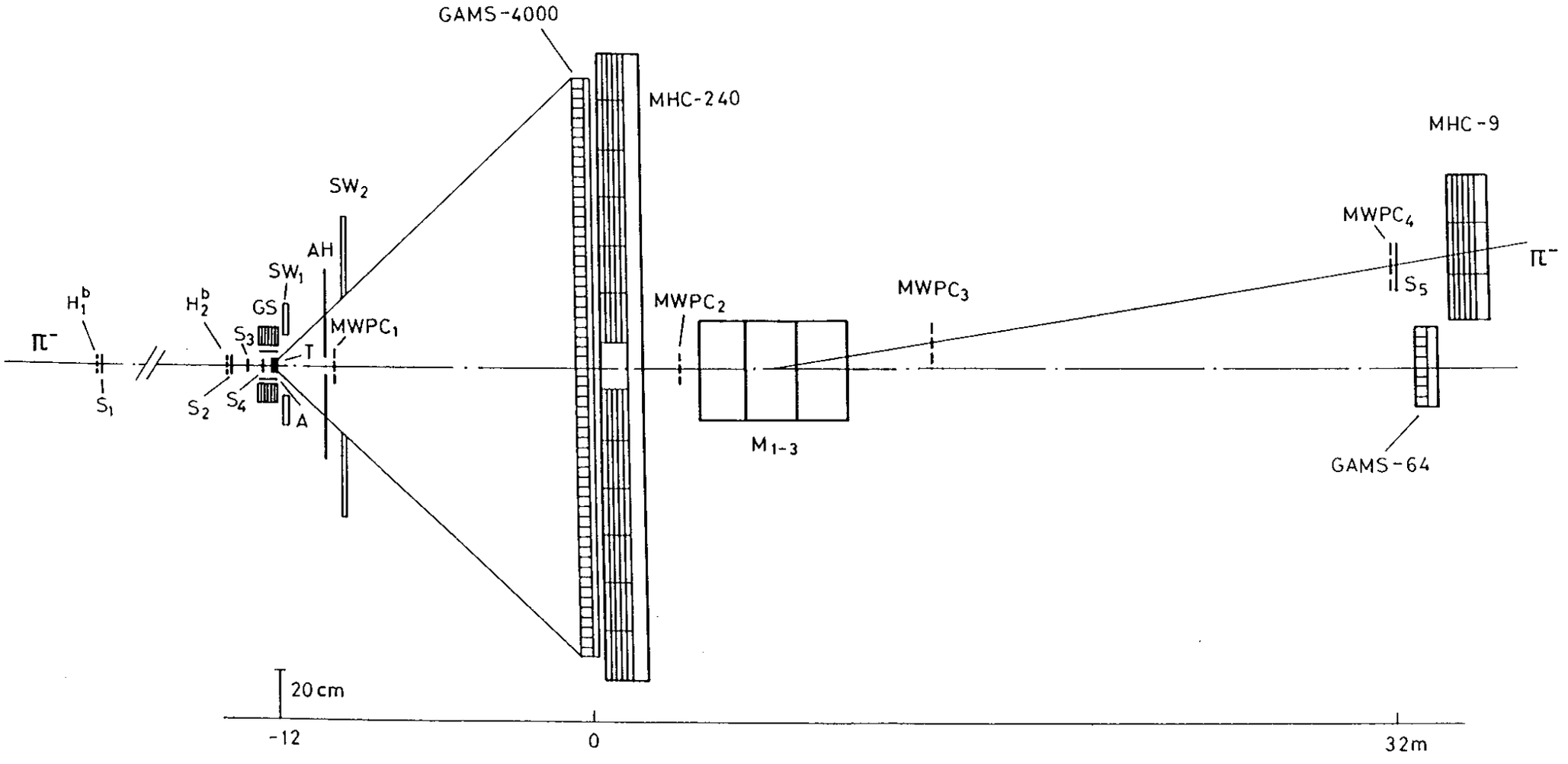
GAMS-4000
MHC-240
MHC-9
SW2
AH
SW1
GS
MWPC1
MWPC2
MWPC3
MWPC4
S5
H1b
H2b
π⁻
S3
T
S1
S2
S4
A
M1-3
GAMS-64
π⁻
20 cm
-12
0
32m

Fig. 1

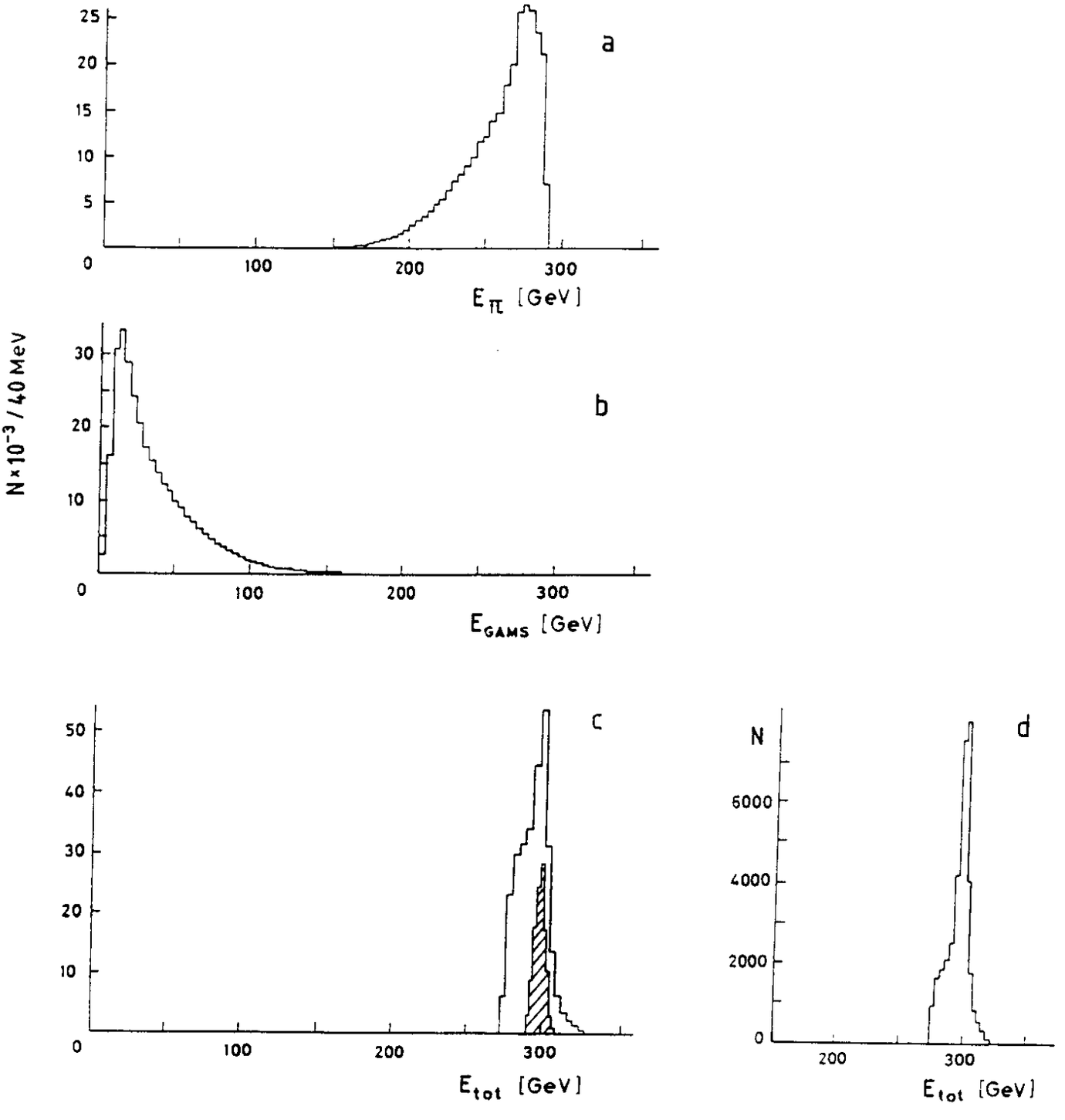
a
25
20
15
10
5
0
100
200
300
$E_\pi$ [GeV]
b
$N \times 10^{-3}$ / 40 MeV
30
20
10
0
100
200
300
$E_{GAMS}$ [GeV]
c
50
40
30
20
10
0
100
200
300
$E_{tot}$ [GeV]
d
N
6000
4000
2000
0
200
300
$E_{tot}$ [GeV]

Fig. 2

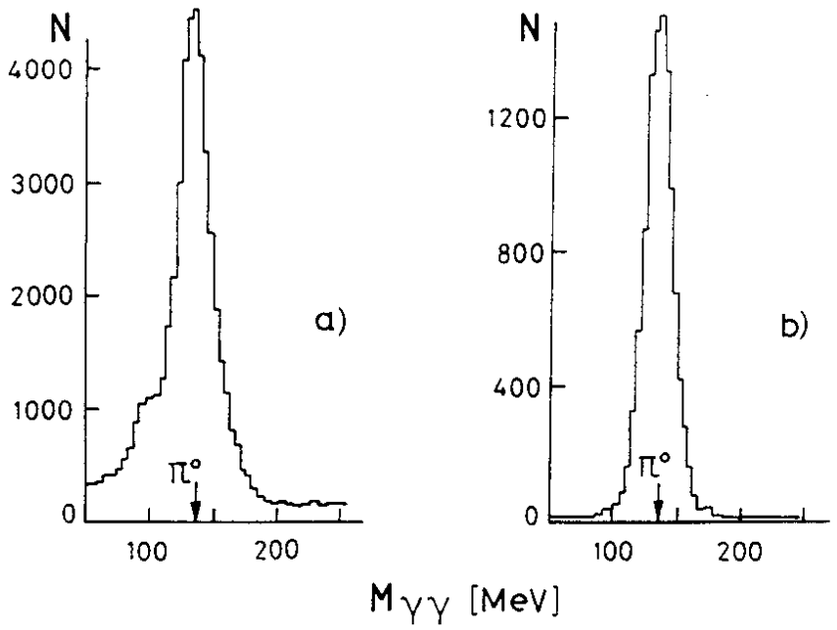
N
4000
3000
2000
1000
0
a)
π°
100
200
N
1200
800
400
0
b)
π°
100
200
Mγγ [MeV]

Fig. 3

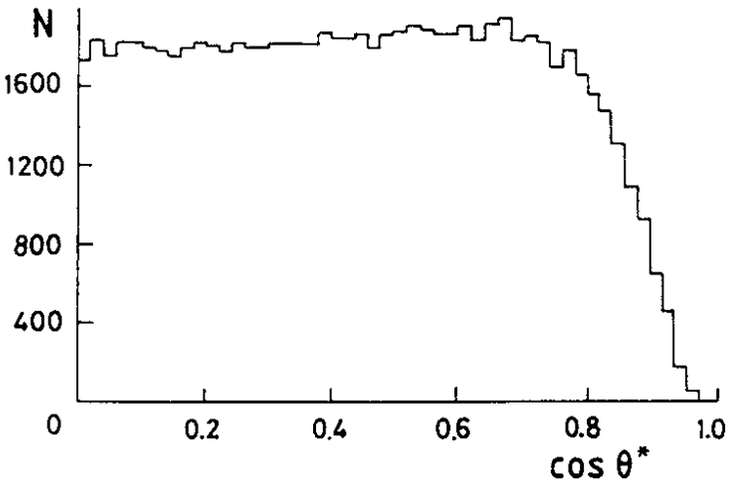
N
1600
1200
800
400
0
0.2
0.4
0.6
0.8
1.0
cos θ*

Fig. 4

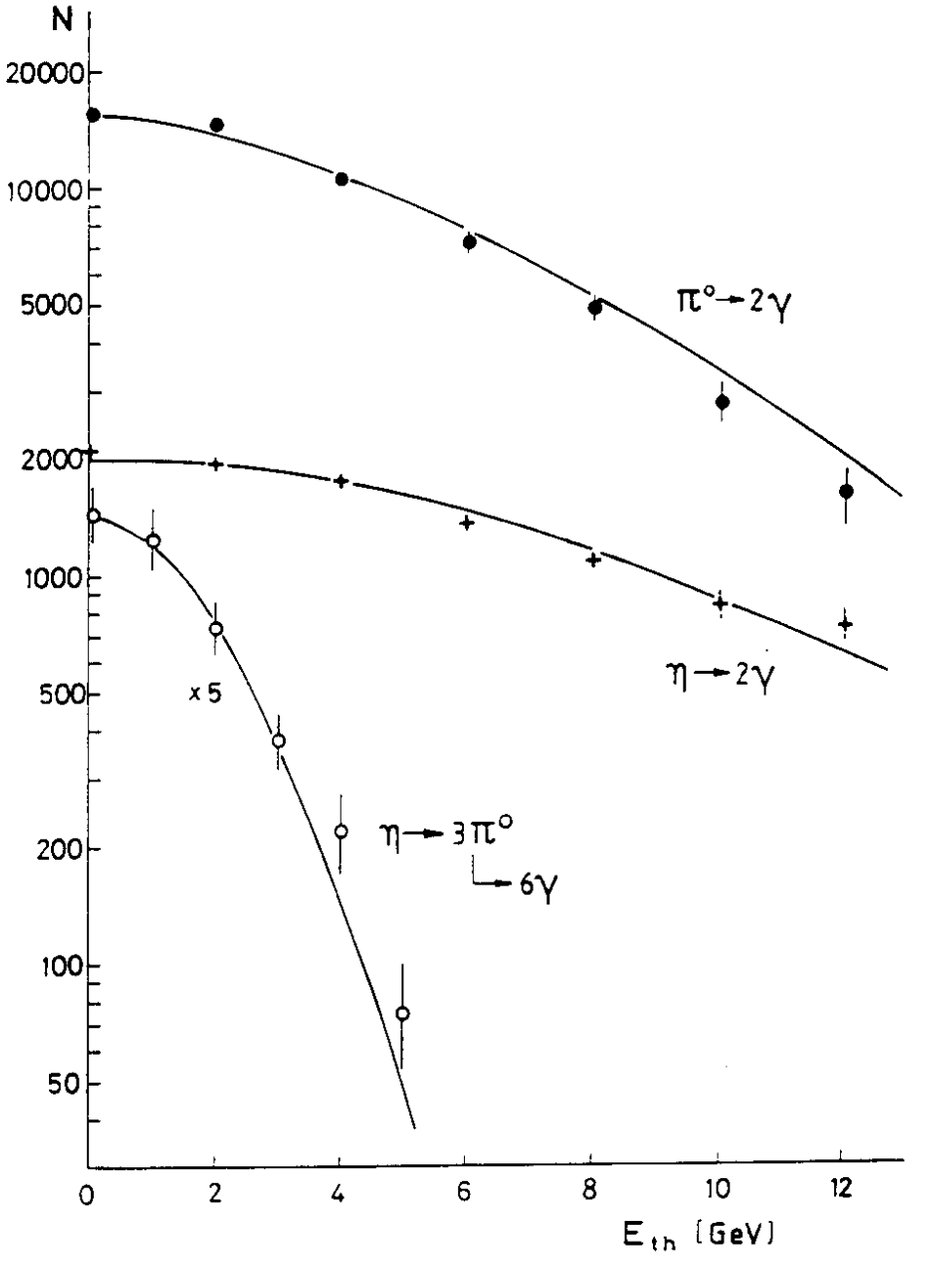
N
20000
10000
5000
2000
1000
500
200
100
50
0
2
4
6
8
10
12
$E_{th}$ [GeV]
$\pi^0 \to 2\gamma$
$\eta \to 2\gamma$
x 5
$\eta \to 3\pi^0$
$\to 6\gamma$

Fig. 5

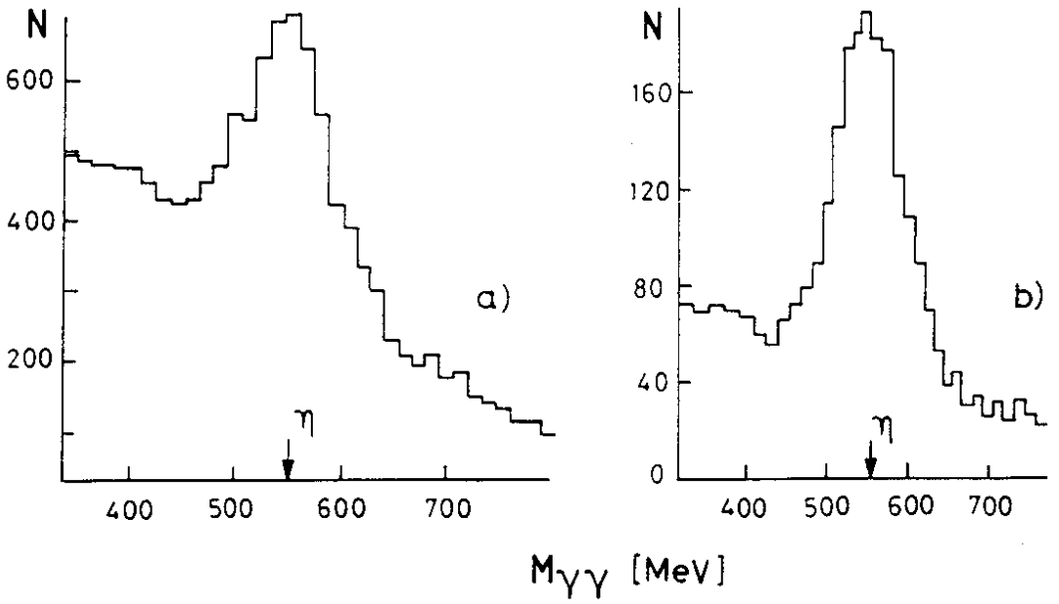
N
600
400
200
a)
η
400
500
600
700
N
160
120
80
40
0
b)
η
400
500
600
700
$M_{\gamma\gamma}$ [MeV]

Fig. 6

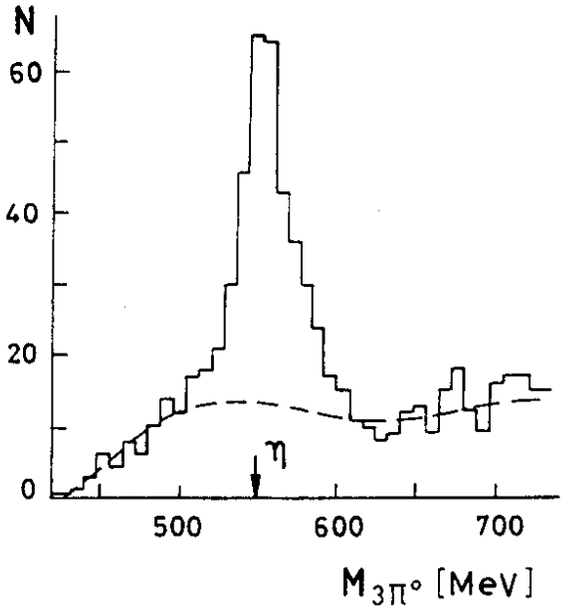
N
60
40
20
0
η
500
600
700
$M_{3\pi^0}$ [MeV]

Fig. 7

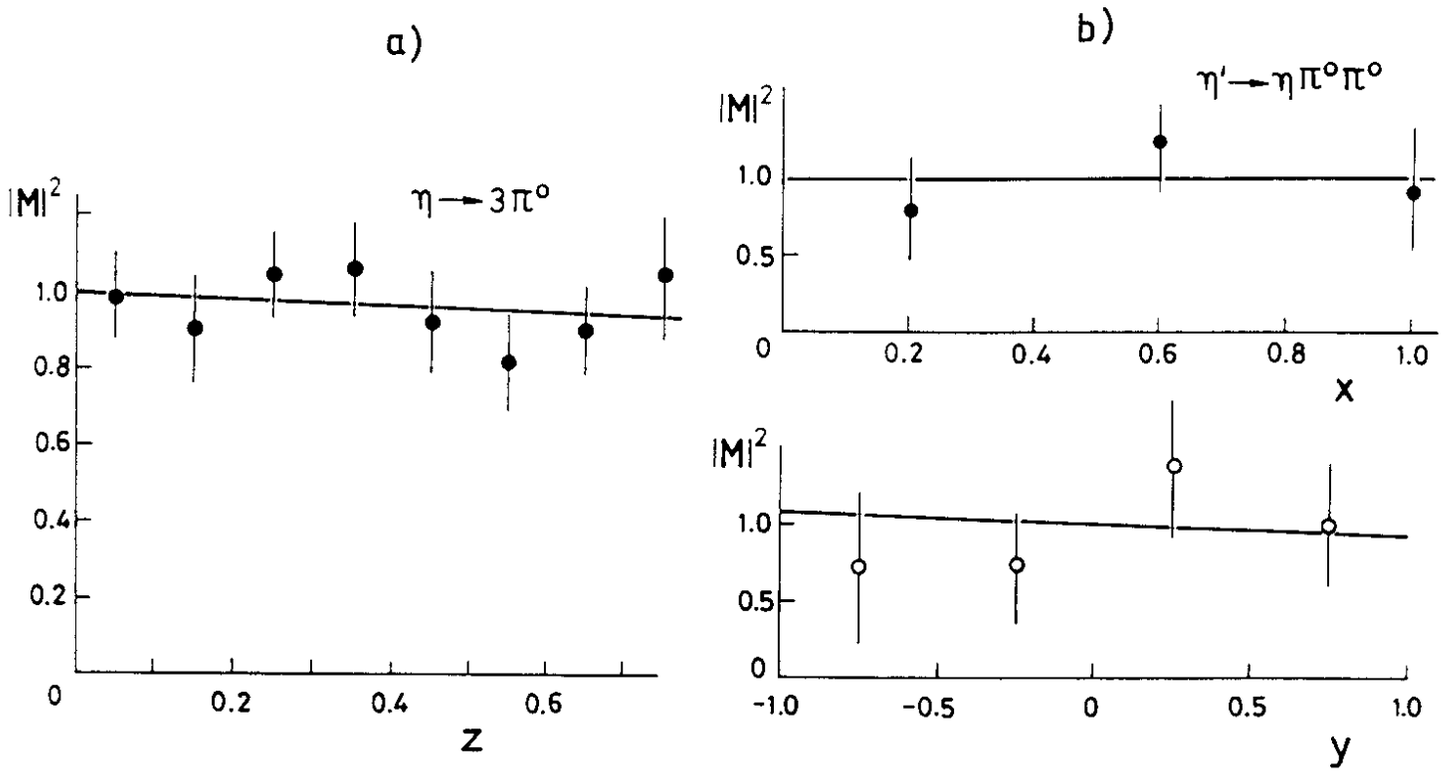


Fig. 8

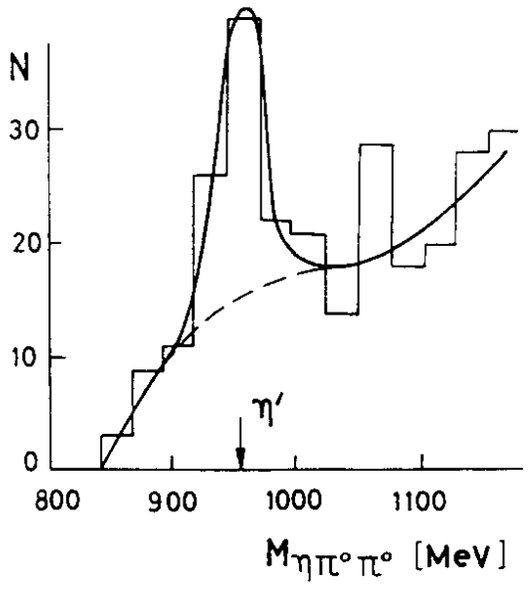


Fig. 9

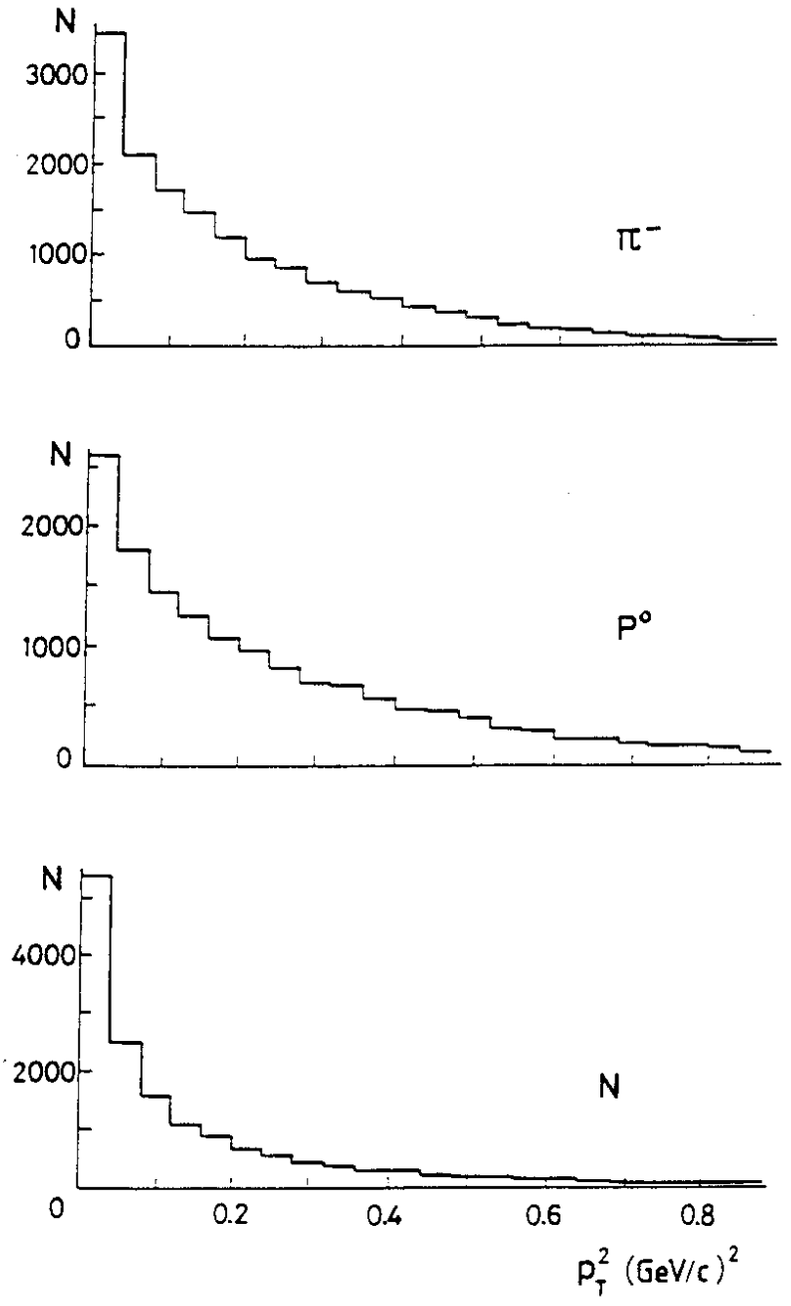
N
3000
2000
1000
0
π⁻
N
2000
1000
0
P°
N
4000
2000
0
N
0.2
0.4
0.6
0.8
$p_T^2$ (GeV/c)$^2$

Fig.10

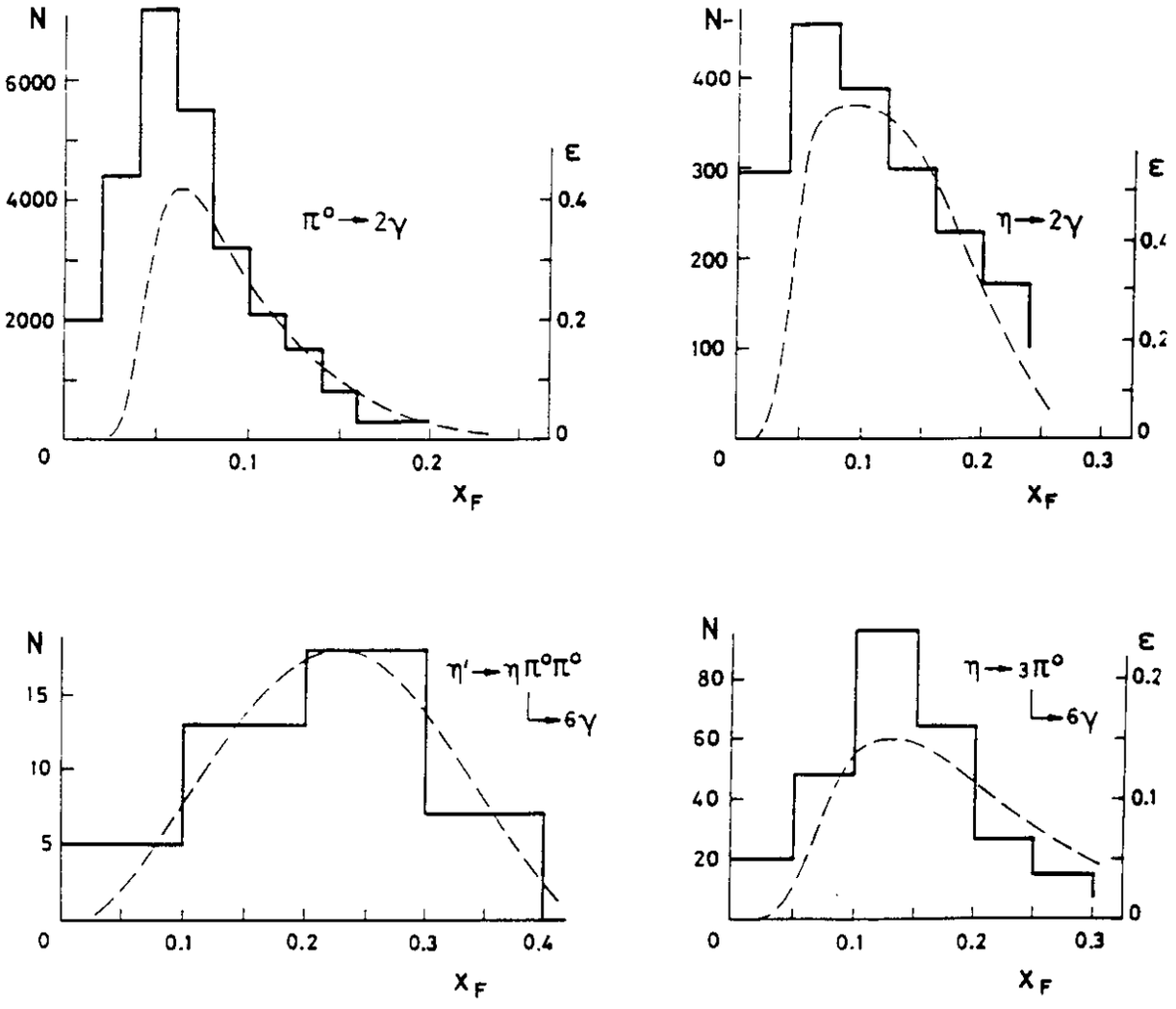
N
6000
4000
2000
0
0.1
0.2
$x_F$
ε
0.4
0.2
0
$\pi^0 \to 2\gamma$
N-
400
300
200
100
0
0.1
0.2
0.3
$x_F$
ε
$\eta \to 2\gamma$
N
15
10
5
0
0.1
0.2
0.3
0.4
$x_F$
$\eta' \to \eta\pi^0\pi^0$
$\to 6\gamma$
N
80
60
40
20
0
0.1
0.2
0.3
$x_F$
ε
0.2
0.1
0
$\eta \to 3\pi^0$
$\to 6\gamma$

Fig. 11